Control-oriented input-delay model of the distributed temperature of a SI engine exhaust catalyst

Delphine Bresch-Pietri, Thomas Leroy and Nicolas Petit

Abstract This chapter aims at showing how a particular class of input delay ordinary differential equations, in which the time- and input-dependent delay is defined through an implicit integral equation, can be used to model accurately the internal temperature of a Spark-Ignited engine catalyst. The modeling approach is grounded on a one-dimensional distributed parameter model, which is approximated by a time-varying first-order delay system whose dynamics parameters (time constant, delay, gains) are obtained through a simple analytic reduction procedure. Following recent works, the distributed heat generation resulting from pollutant conversion is shown here to be equivalent to an inlet temperature entering the system at a virtual front inside the catalyst. The gain of this new input introduces a coupling to account for the conversion efficiency. Relevance of this real-time compliant model is qualitatively supported by experimental data.

1 Introduction

Elements of context. Automotive Spark-Ignited (SI) engines are equipped with a Three-Way Catalyst (TWC) located in the exhaust line. This after-treatment device aims at reducing the three major pollutants resulting from the combustion: hydrocarbons HC, carbon monoxide CO and nitrogen oxide NO_x. Yet, conversion efficiency

Delphine Bresch-Pietri
Department of Mechanical Engineering, Massachusetts Institute of Technology, 77 Massachusetts Avenue, Cambridge MA 02139, USA, e-mail: dbp@mit.edu

Thomas Leroy
Département Contrôle, Signal et Système in IFP Energies nouvelles, 1-4 Av. du Bois Préau, 92852 Rueil Malmaison, France e-mail: thomas.leroy@ifpen.fr

Nicolas Petit
Centre Automatique et Systèmes, Unité Mathématiques et Systèmes at MINES ParisTech, 60 Bd St Michel, 75272 Paris, France e-mail: nicolas.petit@mines-paristech.fr

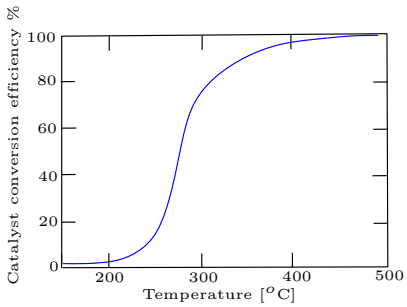

Fig. 1 Conversion efficiency (jointly for CO, HC and NO_x) as a function of temperature for typical catalytic converter (Source: [9]).

highly depends on the catalyst temperature [1] [9] [10], as presented in Fig. 1. Right after a cold start of the engine, temperatures are too low to activate chemical reactions and the catalyst conversion ratio is poor [18]. Therefore, speed-up of the catalyst warm-up is a point of critical importance to reach high level of pollutant conversion.

Classically, warm-up strategies are performed by increasing the exhaust gas temperatures via combustion timing shifting [8]. This open-loop technique leads to a faster heating of the catalyst but also yields combustion efficiency degradation and therefore substantial consumption increase. This increase must be limited to its strict minimum. For this reason, it is of prime importance to determine when the catalyst has reached its light-off temperature[2] to obtain a satisfactory compromise between pollutant emissions and consumption. When this light-off temperature is obtained, standard combustion can be performed and the consumption can simply go back to a standard level.

Motivations for real-time wall temperature modeling. Sadly, no temperature sensor is commercially embedded to provide an information on the distributed wall temperature. In commercial line products, determination of the switch time is currently achieved from the measurements provided by a commercially embedded temperature sensor located into the cooling system. Indeed, the thermal behavior of the water cooling system can be indirectly related to the engine and exhaust line temperatures. Yet, this information is highly uncertain and has no reason to be repeatable (which cannot be allowed anymore as driving cycles tend do diversify).

An alternative is to rely on models. Unfortunately, catalyst temperature models that have been proposed in the literature are either mean-value (spatially lumped) model [11], which do not take into account the inherent distributed nature of the catalyst and can therefore reveal highly inaccurate, or Partial Differential Equations (PDE) modeling [5, 12, 15] with complex representations of the heat release by chemical reactions, which give very accurate estimation of the light-off tempera-

[1] It also highly depends on the Air/Fuel Ratio, the influence of which is not considered here.

[2] Defined here as the temperature at which the catalyst becomes more than 90 percent effective.

ture but are discarded from real-time implementations by the induced computational burden.

Contribution and organization of the chapter. In this chapter, we propose to use a semi-lumped model of these PDE equations. Following the overture presented in [13], we show how a first-order input-delay dynamics relates the inlet gas temperature to a punctual wall catalyst temperature. The obtained model belongs to a particular class of time- and input-dependent delay systems in which the delay is defined through an implicit integral equation which is representative of transport phenomena [17, 21, 23]. The chemical reactions inside the catalyst are simply represented as a fictitious second temperature front entering the catalyst afar off the physical catalyst inlet. This model is shown to be quite accurate, and of gentle implementation complexity.

The model presented here can be seen as a generalization of [13] to SI engines applications. The main modifications consists in the introduction of the catalyst conversion efficiency impacting the heat release. This efficiency depends on the output of the model, resulting into an additional coupling which does not tamper with the stability of the model.

This chapter is organized as follows. Section 2 presents the catalyst under consideration in experiments. In Section 3, we detail the PDE temperature modeling which is used in Section 4 to derive a first-order input-delay model through analytic formula stemming from simple operational calculus. Relevance of the proposed model is discussed at the light of simulations performed on experimental data. We conclude with directions of future works such as prediction-based control strategy.

2 Experimental set-up

The catalyst under consideration in this study is mounted at the outlet of a 2L four-cylinder turbocharged SI engine, downstream the turbine. Fig. 2 presents a scheme of the catalyst under consideration. It is composed of two separated monoliths [19] which, in the following analysis, for the sake of clarity, are not distinguished. For experimental studies and comparisons, the catalyst has been instrumented with two

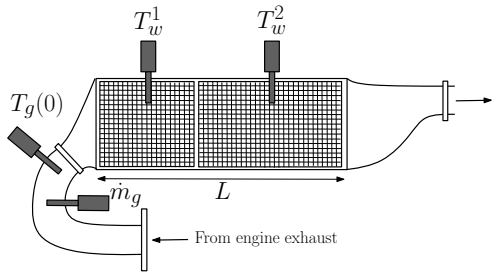

Fig. 2 Experimental catalyst composed of two monoliths. Two sensors permit to measure the wall temperature in the center of each monolith. Test-bench is also equipped with inlet temperature and mass flow sensors.

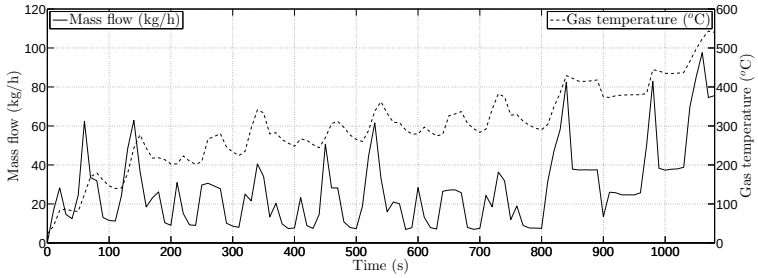

(a) Exhaust gas flow and temperature.

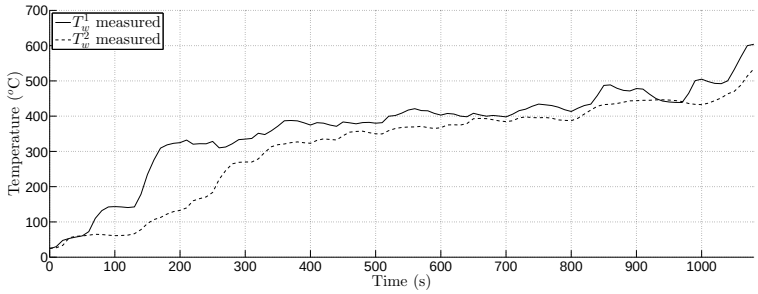

(b) First and second monolith temperature.

Fig. 3 Experimental results on European driving cycle (NEDC).

internal temperature sensors. Such sensors located are not embedded inside any commercial line product. Fig. 3 presents experimental results obtained at test bench during a NEDC (New European Driving Cycle) cycle. Histories of both the exhaust mass flow and the temperature located upstream the catalyst are reported in Fig. 3(a). These quantities are the inputs of the model proposed in this chapter. The exhaust mass flow is a fast-varying variable closely related to the engine torque output. In Fig. 3(b), both monolith temperatures of Fig. 2 are given for a cycle without warm-up strategy. By comparing these two curves between them and against the inlet gas temperature, one can notice the very low-pass filter role of the catalyst (see the signals T_w^1 and T_w^2 on Fig. 3(b)). We will account for this in our model simplification.

3 Partial Differential Equation (PDE) Model

We now refer to Fig. 4, where a schematic representation of the monolith is given. Exhaust burned gas enter the monolith at $x = 0$ and convective exchange with the wall occur all along the monolith, i.e. for $x = 0$ to $x = L$, yielding to distributed temperature profiles of the gas $T_g(x,t)$ and the catalyst wall $T_w(x,t)$ (as underlined in [20, 22], the axial conduction can be neglected).

We consider the following coupled linear infinite dimensional thermal dynamics

$$\begin{cases} \dfrac{\partial T_w}{\partial t}(x,t) = k_1(T_g(x,t) - T_w(x,t)) + \Psi(x,t,T_w(x,t)) & (1) \\ \dot{m}_g \dfrac{\partial T_g}{\partial x}(x,t) = k_2(T_w(x,t) - T_g(x,t)) & (2) \end{cases}$$

where ψ is a distributed time-varying source term, related to the chemical reaction occurring inside the catalyst and the constants $k_1, k_2 > 0$ are defined as

$$k_1 = \frac{h_I P_I}{A_w \rho_w C p_w}, \quad k_2 = \frac{h_I P_I}{C p_g}$$

Notations are gathered in Table 1 in Appendix. Such a model is considered for example in [12]. It encompasses the detailed modeling (14)-(15) given in Appendix, provided that a few simplifications are performed:

- conduction ($\lambda_w \partial^2 T_g / \partial x^2$) into the monolith is neglected compared to convection exchanges;
- gas storage is considered as very small compared to the monolith one, i.e. $\rho_g C p_g << \rho_w C p_w$;
- convective exchanges with the atmosphere are neglected compared to the one with the exhaust gas (this is assumed on for the sake of simplicity of the exposition and can easily be relaxed).

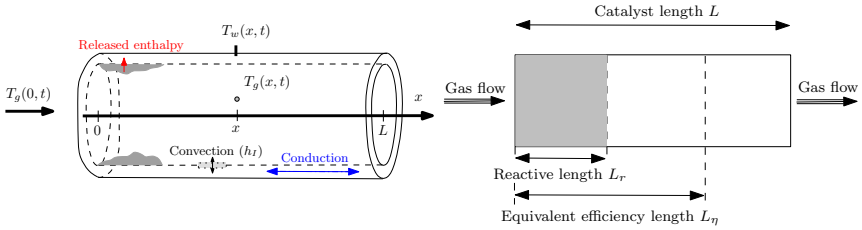

Fig. 4 Schematic views of the distributed profile temperature inside a catalyst jointly with thermal exchanges (left) and of the proposed modeling inspired from [13] (right). The conversion is assumed to take place on an upstream part of the catalyst of length L_r. The temperature used to determine the catalyst efficiency is located at length $L_\eta \leq L$..

The source term ψ gathers the sum of the enthalpies of the various reactions taking place inside the catalyst. It can be effectively represented as

$$\Psi(x,t,T_w) = \begin{cases} \psi(x,t,T_w) & \text{for} \quad 0 \leq x \leq L_r \\ 0 & \text{for} \quad L_r < x \leq L \end{cases}$$

where L_r is the length of the portion of the catalyst where the heat is released. This model is illustrated in Fig. 4. Note that the source term also depends on the wall

temperature. This is important to study the light-off process: for moderate temperature, the conversion efficiency highly depends on the wall temperature and this dependence cannot reasonably be neglected.

In this chapter, we propose to represent the conversion efficiency of the catalyst as a function of a punctual wall temperature, at a position L_η (potentially varying with aging). Experimental determination of this efficiency was performed and follows the tendency of Fig. 1. In the following, it is called η, considered as a known function, and we focus on the design of a simple model of the wall temperature at L_η , handling the potential variability of this position.

4 Approaching the dynamics by an input-delay ordinary differential equation

4.1 Operational calculus without source term

Before detailing the global model that we propose to use, we focus on the analysis of the "purely thermal" behavior of the PDE model, i.e. without any source term. This case is representative of a temperature interval below $250 - 300$, where chemical conversion is almost ineffective.

Claim. Assume $\psi = 0$. In the range of low (time domain) frequencies, the distributed parameter model (1)-(2) can be approximated by the following set of first-order delayed equations

$$\forall 0 \leq x \leq L\,, \quad \tau(x,t)\frac{dT_w(x,t)}{dt} = -\,T_w(x,t) + T_g(0, t - D(x,t)) \quad (3)$$

with

$$\tau(x,t) = \frac{1}{k_1} + \nu\delta(x,t)\,, \quad D(x,t) = (1-\nu)\delta(x,t) \quad (4)$$

where ν is a given constant in $[0,1]$ and δ is defined through the integral equation

$$\int_{t-\delta(x,t)}^{t} \frac{k_1}{k_2}\dot{m}_g(s)ds = x \quad (5)$$

The relation (5) implicitly defines a transport delay through past values of the gas flow rate. It corresponds to a transport phenomenon occurring over a length x with a speed $\frac{k_1}{k_2}\dot{m}_g$ accordingly to a Plug-Flow assumption [17]. This time can be

understood as a residence time into the monolith (see [4]). As the two main effects of the gas residence inside the monolith are transport and exchange with the monolith, it can reasonably be separated into a first order dynamics with a pure delay effect. The tuning parameter ν can be determined via dedicated tests (e.g. given operating points, for which the engine is initially cold and requested torque and engine speed are kept constant) and allows this model to qualitatively represent a relatively vast range of catalyst devices.

4.1.1 Formulation of claim 4.1

Transport delay

By taking a spatial derivative of (1), a time-derivative of (2) and matching terms with (1)-(2), one can obtain the decoupled equations, for all $x \in [0, L]$,

$$\begin{cases} \dot{m}_g(t)\dfrac{\partial^2 T_w}{\partial x \partial t} = -k_2\dfrac{\partial T_w}{\partial t} - k_1\dot{m}_g(t)\dfrac{\partial T_w}{\partial x} \\ \dot{m}_g(t)\dfrac{\partial^2 T_g}{\partial x \partial t} + \ddot{m}_g(t)\dfrac{\partial T_g}{\partial x} = -k_2\dfrac{\partial T_g}{\partial t} - k_1\dot{m}_g(t)\dfrac{\partial T_g}{\partial x} \end{cases}$$

where the first equation defining T_w can be reformulated using a spatial Laplace transform (operational calculus) to get

$$\forall t \geq 0\,, \quad (\dot{m}_g(t)p + k_2)\frac{d\hat{T}_w}{dt} = -k_1\dot{m}_g(t)p\hat{T}_w(p,t)$$

This scalar system can be solved as

$$\hat{T}_w(p,t) = \exp\left(-\left[\int_{t_0}^{t}\frac{k_1\dot{m}_g(s)p}{\dot{m}_g(s)p + k_2}ds\right]\right)\hat{T}_w(p,t_0)$$

where t_0 is such that $t_0 \leq t$. The catalyst, as is visible from experimental data reported in Fig. 3(b), is relatively non-sensitive to high-frequencies. Consequently, by considering only low-level spatial frequencies (i.e., $\dot{m}_g p << k_2$ for any gas flow $\dot{m}_g$), the term below the integral can be substantially simplified. Rewriting the resulting equation into the usual space domain gives

$$\forall x \in [0, L]\,, \quad T_w(x,t) = T_w\left(x - \left[\int_{t_0}^{t}\frac{k_1}{k_2}\dot{m}_s(s)ds\right], t_0\right)$$

Formally, one can define $\delta(x,t) \geq 0$ such that

$$x - \left[\int_{t-\delta(x,t)}^{t}\frac{k_1}{k_2}\dot{m}_s(s)ds\right] = 0$$

which is equivalent to the implicit integral equation (5). Consequently, the wall temperature at abscissa x is formally delayed by

$$\forall x \in [0, L], \quad T_w(x,t) = T_w(0, t - \delta(x,t)) \tag{6}$$

First-order model

From there, it is possible to relate the dynamics under consideration to the gas inlet temperature. Consider for a moment that $\delta(x)$ is constant with respect to time. Then, writing (6) in the time Laplace domain, jointly with (1) for $x = 0$, one directly obtains for all $x \in [0, L]$

$$\hat{T}_w(x,s) = k_1 \frac{e^{-\delta(x)s}}{s + k_1} \hat{T}_g(0,s) \tag{7}$$

Finally, following the same steps as previously, it is possible to only consider low frequencies ($s << 1$). By following the elements presented in [16],

$$e^{-\delta(x)s} \approx \frac{e^{-(1-\nu)\delta(x)s}}{\nu\delta(x)s + 1}$$

with a constant $\nu \in [0, 1]$, (7) rewrites for low frequencies as

$$\hat{T}_w(x,s) = \frac{e^{-(1-\nu)\delta(x)s}}{\left(\frac{1}{k_1} + \nu\delta(x)\right) s + 1} \hat{T}_g(x,0)$$

By formally generalizing this relation to a time-varying residence time $\delta(x,t)$, one obtains the dynamics formulated in Claim 4.1.

4.1.2 Validation of the reduced model (3)-(5) using experimental data

To illustrate Claim 4.1, simulation results of the temperature inside the wall catalyst at two different locations are pictured in Fig. 5. The two simulation results have been obtained respectively with the distributed parameter model (1)-(2) (with $\psi = 0$, i.e. neglecting the enthalpy flows) and with the proposed simplified dynamics (3)-(5). The inputs used for the two models (gas mass flow rate and gas inlet temperature) are data recorded during a NEDC cycle. They are pictured in Fig. 3(a).

Implementation of the proposed model was performed with a forward Euler approximation of (3). The value of δ is determined based on a trapezoidal approximation of (5) with a simple calculation procedure: the integral left-hand side of (5) is an increasing function of δ, equal to zero for $\delta = 0$; therefore, we calculate it recursively for increasing values of δ, starting with $\delta = 0$, stopping when reaching or passing x.

The simulated temperature in Fig. 5 almost perfectly matches the one computed with the PDE model. As these performances are obtained for very demanding external conditions (large gas mass flow rate variations), one can reasonably expect

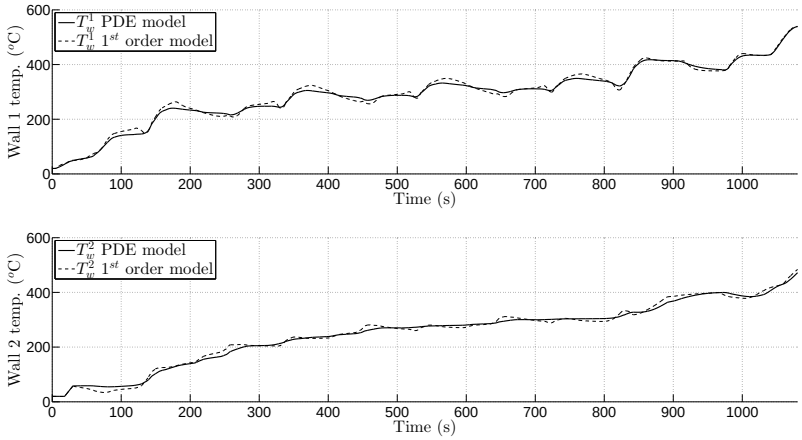

Fig. 5 Simulation comparison between the temperature representation of the model (1)-(2) with $\psi = 0$ and the reduced first-order input-delay model (3)-(5). The inputs of the model are NEDC variations pictured in Fig. 3(a).

similar behavior on different kinds of driving conditions. For typically encountered input signals, the PDE model is well represented by the model of Claim 4.1.

Nevertheless, these models cannot completely match experimentally measured data, as the heat released from chemical reactions is neglected. We now investigate this point.

4.2 Including chemical reactions energy

To account for the source term ψ, we propose to consider the pollutant conversion effects as a second temperature front T_{eq} occurring at virtual position L_r inside the catalyst [3]. This model allows one to exploit the linearity of the dynamics (3)-(5), through a superposition principle, to distinguish the $T_g(0)$ effects from the pollutant conversion effect. This model approach is pictured on Fig. 6.

For steady-state conditions, energy balance for the system can be written as

$$\dot{m}_g Cp_g \underbrace{(T_g(0) - T_g(L))}_{\triangleq T_{eq}} + \eta(T_w(L_\eta)) \sum_{i=1}^{N} \Delta H_i [x_i]_{in} = 0$$

where $[x_i]_{in}$ are the inlet pollutant concentrations. Typically, three main pollutants are considered ($N = 3$), i.e. hydrocarbons (HC), carbon monoxide (CO) and nitrogen oxides (NO_x). They result in three steady-state gains

[3] In details, this fictitious length does not exactly match the physical non-reactive length introduced earlier in Section 3. Yet, for sake of simplicity, we assume here that they are identical.

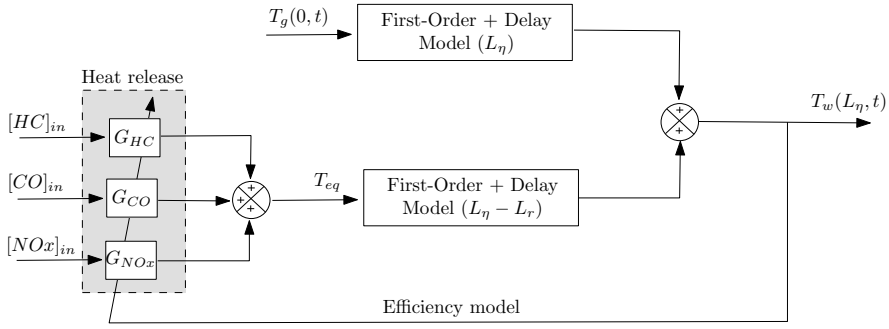

Fig. 6 Proposed catalyst temperature model (9)-(13). The pollutant conversion effects (HC, CO and NO_x) are assimilated to a front of temperature T_{eq} propagating on a virtual length $L_\eta - L_r$, while the gas heating occurs on the complete length L_η. The model is also fed by the gas mass flow rate $\dot{m}_g$ which is not represented here for sake of clarity.

$$G_{HC} = \eta(T_w(L_\eta))\frac{\Delta H_{HC}}{\dot{m}_g Cp_g}, \quad G_{CO} = \eta(T_w(L_\eta))\frac{\Delta H_{CO}}{\dot{m}_g Cp_g}$$
$$\text{and} \quad G_{NO_x} = \eta(T_w(L_\eta))\frac{\Delta H_{NO_x}}{\dot{m}_g Cp_g}$$

where the unity enthalpy $\Delta H_{HC}, \Delta H_{CO}$ and ΔH_{NO_x} are known constants. These gains are then used to calculate an equivalent temperature

$$T_{eq} = G_{HC}[HC]_{in} + G_{CO}[CO]_{in} + G_{NO_x}[NO_x]_{in} \tag{8}$$

In practice, the pollutant concentrations are not measured but can be effectively estimated, e.g. by look-up tables.

An important point to notice is the appearance of the temperature at length L_η as a parametrization of the conversion efficiency. This yields a coupling represented in Fig. 6 under a closed-loop form.

We summarize this approach by the following claim.

Claim. For any source term ψ, the wall catalyst temperature at position L_η can be efficiently represented as

$$T_w(L_\eta) = T_w^{th} + T_w^{\psi} \tag{9}$$

where T_w^{th} satisfies

$$\tau(L_\eta, t)\frac{dT_w^{th}}{dt} = -T_w^{th}(t) + T_g(0, t - D(L_\eta, t)) \tag{10}$$

and T_w^{ψ} satisfies

$$\tau(L_\eta - L_r, t)\frac{dT_w^\psi}{dt} = -T_w^\psi(t) + T_{eq}(0, t - D(L_\eta - L_r, t)) \tag{11}$$

T_{eq} is defined in (8), the time constant τ and the delay D are defined for $x \in [0, L]$ as

$$\tau(x,t) = \frac{1}{k_1} + \nu\delta(x,t)\,, \quad D(x,t) = (1-\nu)\delta(x,t) \tag{12}$$

with ν a given constant in $[0, 1]$ and δ defined through the integral equation

$$\int_{t-\delta(x,t)}^{t} \frac{k_1}{k_2}\dot{m}_g(s)ds = x \tag{13}$$

It is worth noticing that the catalyst temperature at any position $x \in [0, L]$ can also be computed by a similar procedure, provided one has value of the steady-state gains (correspondingly, $T_w(L_\eta, .)$ has to be calculated independently).

4.3 Validation of the proposed model on experimental data

Simulation results of the wall catalyst temperature at two positions (described in Fig. 2) are provided in Fig. 7 and compared to experimental measurements. These measurements were obtained on a NEDC cycle, with an initially cold catalyst. The tuning parameter is set to $\nu = 0.4$.

One can easily notice that the computed temperatures catch both short-term and long-term variations of the true signals. As previously, it is worth noticing that the inputs corresponding to this NEDC cycle are highly variable and therefore this test case is challenging.

The proposed model is simple enough to be implemented in real-time and provides accurate estimation of the wall catalyst. One clear advantage of the proposed technique that is worth noticing is that it provides insight into the temperature everywhere inside the monolith. A lumped model (or 0D-model) like the one presented in [11] for example, cannot achieve this. Also worth noticing is the fact that aging of the catalyst can be accounted for by updating L_η.

To feed the model, values for various inputs, presented in Fig.6, are necessary: the mass flow rate (already modeled for cylinder charge estimation and combustion control), the inlet gas temperature (the modeling of which has been widely investigated in the literature, see [6, 7]) and the pollutant emissions upstream of the catalyst.

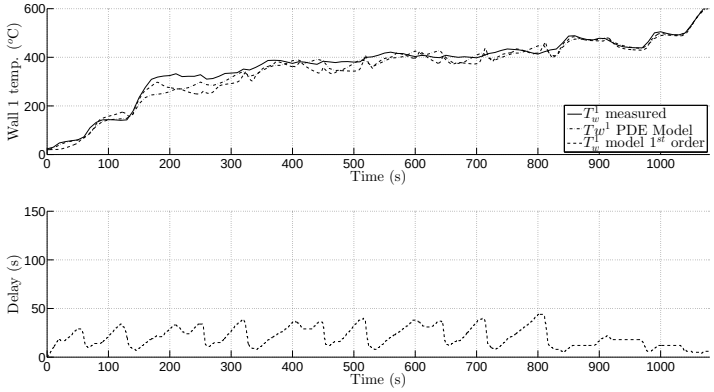

(a) Simulation results for the first-order input-delay model approach, compared to experimental data in the center of the first monolith, and the corresponding delay used in the model.

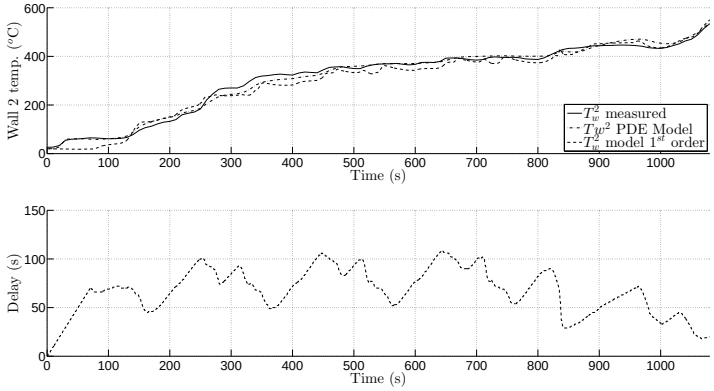

(b) Simulation results for the first-order input-delay model approach, compared to experimental data in the center of the second monolith, and the corresponding delay used in the model.

Fig. 7 Comparison between the proposed model and experimental data at two location inside the monolith.

5 Conclusion

In this chapter, a simple infinite dimensional model of the wall catalyst has been presented and a corresponding first-order input-delay reduction has been performed. Besides its real-time compliance, this model also exhibits the interesting property of providing an estimation of the wall temperature without requiring additional offline tuning procedures.

This reduced input-delay model is of particular interest to design strategies which, compared to the existing ones, enable to detect light-off independently on the driving cycle (see [2] for further experimental-based simulation illustrating this point). Other control strategies exploiting the delay representation such as the

prediction-based techniques proposed in [3] can also be considered. Further evaluation of their potential merits is the scope of future work. Another direction of work is the evaluation of the robustness of this model to input estimation errors (in particular with respect to inlet pollutant emissions which are not measured but obtained through look-up tables).

Appendix

In this appendix, we provide a more detailed modeling of the thermal exchanges occurring in the catalyst, from which (1)-(2) is a simplification. Following [5], a thermal balance of the gas leads to the equation

$$\rho_g A_g C p_g \frac{\partial T_g}{\partial t} + \dot{m}_g C p_g \frac{\partial T_g}{\partial x} = h_I P_I (T_w(x,t) - T_g(x,t)) \tag{14}$$

where the first term on the left hand side accounts for the gas energy storage, the second one for transport and the right-hand term for convective exchanges. A similar balance for the wall yields

$$\begin{aligned} \rho_w A_w C p_w \frac{\partial T_w}{\partial t} =& \lambda_w \frac{\partial^2 T_w}{\partial x^2} + \sum_{i=1}^{N} R_i h_i + h_I P_I (T_g(x,t) - T_w(x,t)) \\ &+ h_O P_O (T_{amb} - T_w(x,t)) \end{aligned} \tag{15}$$

where the left-hand side still accounts for the energy storage and the right-hand side represents respectively: i) the conduction/diffusion inside the monolith; ii) the enthalpy flow of the N chemical reactions occurring inside the catalyst (mainly, $N = 3$); iii) the exchange respectively with the gas and the atmosphere.

One can notice that, following [13], no transport occurs in the (solid) wall. In more details, a mass balance of the species in presence can be established. The species concentrations inside the monolith are necessary to determine the reaction terms R_i in the enthalpy flows. Two additional equations per species are also necessary (one for the gas and one for the monolith, see [1] [14]).

References

1. S. F. Benjamin and C. A. Roberts. Automotive catalyst warm-up to light-off by pulsating engine exhaust. *International Journal of Engine Research*, 5(2):125–147, 2004.
2. D. Bresch-Pietri, T. Leroy and N. Petit Control-oriented time-varying input-delayed temperature model for SI engine exhaust catalyst in *Proc. of the American Control Conference*, 2013
3. D. Bresch-Pietri, T. Leroy and N. Petit Estimation of the distributed temperature of a SI engine catalyst for light-off strategy in *Proc. of the European Control Conference*, 2013
4. P. V. Danckwerts. Continuous flow systems: distribution of residence times. *Chemical Engineering Science*, 2(1):1–13, 1953.
5. C. Depcik and D. Assanis. One-dimensional automotive catalyst modeling. *Progress in energy and combustion science*, 31(4):308–369, 2005.
6. L. Eriksson. Mean value models for exhaust system temperatures. In *Proc. of the Society of Automotive Engineering World Congress*, number 2002-01-0374, 2005.

Symbol	Description	Unit	Symbol	Description	Unit
A_w	Catalyst wall area	m^2	$\dot{m}_g$	Gas mass flow rate	kg/s
A_g	Catalyst efficient area	m^2	P_I	Internal catalyst perimeter	m
Cp_w	Catalyst wall heat capacity	J/kg/m^3	P_O	External catalyst perimeter	m
Cp_g	Gas heat capacity	J/kg/m^3	R_i	Reaction rate of the i^{th} species	-
D	Model delay	s	ρ_w	Catalyst wall volumetric mass	kg/m^3
ΔH_{HC}	Unity enthalpy from HC conversion	J/mol	T_w	Distributed monolith temperature	K
ΔH_{CO}	Unity enthalpy from CO conversion	J/mol	T_w^1	Wall temperature in the middle of the first monolith	K
ΔH_{NOx}	Unity enthalpy from NO_x conversion	J/mol			
h_I	Internal convection coefficient	J/K/m^2	T_w^2	Wall temperature in the middle of the second monolith	K
h_O	External convection coefficient	J/K/m^2			
h_i	Enthalpy of the i^{th} species reaction	J	T_g	Distributed gas temperature	K
λ_w	Wall conduction coefficient	J/K/m^2	τ	Model time constant	s

Table 1 Notations

7. H. Fu, X. Chen, I. Shilling, and S. Richardson. A one-dimensional model for heat transfer in engine exhaust systems. In *Proc. of the Society of Automotive Engineering World Congress*, number 2005-01-0696, 2005.
8. L. Guzzella and C. H. Onder. *Introduction to Modeling and Control of Internal Combustion Engine Systems*. Springer Verlag, 2010.
9. J. B. Heywood. *Internal Combustion Engine Fundamentals*. McGraw-Hill New York, 1988.
10. U. Kiencke and L. Nielsen. *Automotive Control Systems*. Springer-Verlag, Berlin, 2000.
11. D. Kum, H. Peng, and N. K. Bucknor. Optimal energy and catalyst temperature management of plug-in hybrid electric vehicles for minimum fuel consumption and tail-pipe emissions. *IEEE Transactions on Control Systems Technology*, 21(99):14–26, 1999.
12. P. M. Laing, M. D. Shane, S. Son, A. A. Adamczyk, and P. Li. A simplified approach to modeling exhaust system emissions: SIMTWC. *SAE paper*, -:01–3476, 1999.
13. O. Lepreux. *Model-based temperature control of a Diesel oxidation catalyst*. PhD thesis, MINES Paristech, 2010.
14. L. Olsson and B. Andersson. Kinetic modelling in automotive catalysis. *Topics in catalysis*, 28(1):89–98, 2004.
15. A. Onorati, G. D'Errico, and G. Ferrari. 1D fluid dynamic modeling of unsteady reacting flows in the exhaust system with catalytic converter for SI engines. *SAE Transactions*, 109(2000-01-0210):89–103, 2000.
16. L. Pekar and E. Kureckova. Rational approximations for time-delay systems: case studies. In *Proc. of the Conference on Mathematical and computational Methods in Science and Engineering*, 217–222, 2011.
17. R. H. Perry, D. W. Green, and J. O. Maloney. *Perry's Chemical Engineers' Handbook*, volume 7. McGraw-Hill New York, 1984.
18. C. P. Please, P. S. Hagan, and D. W. Schwendeman. Light-off behavior of catalytic converters. *SIAM Journal on Applied Mathematics*, 54(1):72–92, 1994.
19. K. Ramanathan, D. H. West, and V. Balakotaiah. Optimal design of catalytic converters for minimizing cold-start emissions. *Catalysis today*, 98(3):357–373, 2004.
20. J. Vardi and W. F. Biller. Thermal behavior of exhaust gas catalytic convertor. *Industrial & Engineering Chemistry Process Design and Development*, 7(1):83–90, 1968.
21. M. Wu, C. Wang, W. Cao, X. Lai, and X. Chen. Design and application of generalized predictive control strategy with closed-loop identification for burn-through point in sintering process. *Control Engineering Practice*, 20:1065–1074, 2012.
22. L. C. Young and B. A. Finlayson. Mathematical models of the monolith catalytic converter. *AIChE Journal*, 22(2):343–353, 1976.
23. K. Zenger and R. Ylinen. Simulation of variable delays in material transport models. *Mathematics and computers in simulation*, 37:52–72, 1994.